Raman characterization of plastics: a DFT study of polystyrene

Beata Taudul[1], Frederik Tielens[2], Monica Calatayud[1]*

[1] Sorbonne Université, CNRS, Laboratoire de Chimie Théorique, LCT, 4 Place Jussieu, F-75005 Paris, France ; beata.taudul@gmail.com

[2] Department of General Chemistry (ALGC) – Materials Modelling Group, Vrije Universiteit Brussel, Pleinlaan 2, 1050 Brussel, Belgium; frederik.tielens@vub.be

* Correspondence: monica.calatayud@sorbonne-universite.fr; Phone: +33 01 44 27 25 05

Abstract

Plastic materials are massively present in technological, industrial, and everyday applications, with increasing concern in toxicological aspects for health and environment. Characterization becomes an important issue as the structural, size and textural properties of plastics are needed to identify and track their life, from their production to their eventual degradation. Raman spectroscopy appears as a key tool for characterizing a wide variety of materials including plastics. It is fast, robust, sensitive to nanosized and amorphous particles. In order to be properly used for plastics, the Raman response of reference materials needs to be carefully assessed, the literature on such assessments being scarce. In this work, we attempt to fill this gap by employing theoretical calculations to generate *ab initio* spectra on the reference material polystyrene. The goal is to explain the origin of the peaks and their robustness to map the Raman response on controlled composition and structure, using linear ordered polymeric and finite amorphous models. The CRYSTAL package has been used to obtain full Raman spectra (vibrations, intensity) based on a careful benchmark of computational settings of functional and basis set. Whereas some peaks are found to be present in all the spectra and could be used for calibration purposes, other peaks are structure dependent and could be used to identify the type of polymer. We conclude that Raman spectroscopy is a technique well suited for the study of plastics, provided that a careful analysis of the origin of signal is done to fully interpret the spectra and deploy applications.

I. INTRODUCTION

Production of plastic has been continuously increasing since the 1950s, with common types like polystyrene, polypropylene, polyethylene terephthalate, and polyvinyl chloride, being widely used in mass production [1,2]. Unfortunately, this massive global plastic production has led to a significant pollution problem in recent years and due to its slow degradation rate plastic contributes to the accumulation of large amounts of plastic waste in the natural environment [3–5]. As a consequence, plastics are involved in a cycle that affects the atmosphere, terrestrial system, and aquatic system, with all these systems being interconnected [6–9]. The smallest plastic particles, such as microplastics (<5 mm in diameter [10]) and nanoplastics (1 μm–1 nm [11]), are the ones that cycle through these systems the most.

These tiny plastic particles pose contamination risks throughout the trophic chain, affecting all levels of the food chain, and there are growing concerns about its impacts on marine life and human health [12–16]. Spectroscopic techniques, particularly Raman and Fourier transform infrared (FTIR) spectroscopy, are widely used in microplastic studies to characterize plastic particles [16–21]. In fact, Raman spectroscopy is becoming a key technology used in research and development for characterization of nanomaterials, widely used for diverse applications like heterogeneous catalysis, plastic detection, cellular investigation or medicine [22–27]. It is a non-destructive technique that provides information on the structure of a material, type of species and chemical bonds, and it is particularly well suited to study nanosized materials, for which common characterization techniques based on microscopy or diffraction cannot be applied. Raman spectroscopy has been successfully applied to characterize microplastics [28–37], and offers some advantages over FTIR. Among others, Raman techniques show higher spatial resolution, wider spectral coverage, higher sensitivity to non-polar functional groups, lower water interference and narrower spectral band [38,39].

In order to be properly applied, Raman spectrometers need a first calibration step where the signal is aligned with reference materials. Polystyrene (PST) is one of the common calibration samples due to its low cost and signal behavior [40]. Its polymeric nature implies a large number of compositional parameters that can affect its Raman response: phenyl group orientation, chains length, branching, density, impurities, chain termination… A detailed understanding of the role that each of these factors have on the Raman spectrum is necessary to assess the use of PST as calibration material and the characterization of plastics composition and structure. Whereas it is experimentally difficult to prepare samples with full control on those parameters, modelling provides a rich playground to analyze structural effects in the Raman response, among others. In this work we will perform an *ab initio* theoretical investigation of the Raman spectra of PST selected models to elucidate the structural factors affecting the corresponding Raman spectrum, and will discuss the validity of PST as reference material in the calibration of Raman equipment.

Polystyrene can be synthesized in different tactic forms, that differ in the arrangement of phenyl rings with respect to the carbon chain, that affect its properties and potential applications [41]. Among these forms, syndiotactic polystyrene (sPST), with phenyl groups positioned on alternating sides of the hydrocarbon backbone, poses valuable physical and mechanical properties such as high melting point, excellent chemical stability and fast crystallization rate, that make it well suited to be used as calibration material [40–43]. In a crystalline form sPST shows various polymorphic structures and depending on the preparation conditions, the crystal type, morphology and associated physical properties of sPST can be modified [41–47]. Consequently, four main crystalline forms of sPST can be identified and denoted as α, β, γ and δ. The most stable α (hexagonal) and β (orthorhombic) forms of sPST show a *trans*-planar (zigzag) [TTTT] conformation of carbon chain, with an identity period of $c(\beta) \approx 5.06$ Å and $c(\alpha) \approx 5.1$ Å [42,43]. On the other hand, the γ and δ forms, that can be induced by solvents during crystallization, have monoclinic structure and exhibit the s(2/1)2 helical chain conformation [TTGG], with an identity period of $c(\delta) \approx 7.71$ Å [42,43]. The *trans*-planar and helical conformations of sPST chains are schematically shown in Figure 1.

The Raman spectra of syndiotactic polystyrene have been widely measured and interpreted to date [48–53], but a limited number of theoretical studies exist, and only a few examples of calculated vibrational spectra of polystyrene can be found [50,51,54]. Vibrational modes and full IR spectra were evaluated for single infinite chains of trans-planar and s(1/2) helical forms of PST, and detailed analysis of vibrational modes was performed allowing to

assign each mode to corresponding vibrating groups of atoms. Yet, the calculation of Raman intensities was not computationally affordable until recently, and full theoretical Raman spectra of polystyrene is missing. Moreover, the available studies considered infinite polystyrene chains with well-defined rod group symmetries [50,51]. These works provide valuable information about the vibrational properties of polystyrene; in particular the use of symmetries and character tables allows for detailed vibrational mode analysis. However, those ideal models can be improved to mimic more realistic conditions.

In the presented paper, we aim to partially fill this gap by producing Raman spectra of more complex structural models that would be closer to real samples, focusing mainly on the polystyrene conformation. In particular, we will consider infinite trans-planar and helical chains of sPST, together with short polystyrene oligomers of finite chain lengths with linear and bent carbon backbone structure. Our selection will account therefore for relative phenyl distribution along PST chains, chain termination and disorder, and will provide rich information about both the position and the intensity of Raman peaks. It is important to highlight that our calculations do not include the crystalline polymorph structures of sPST. Instead, our primary focus is to understand the impact of the polymer configuration itself. Therefore, we concentrate on isolated chains of trans-planar and helical sPST that should include the most relevant vibrational modes of the α/β and γ/δ phases of sPST, respectively.

Raman spectra are calculated by means of density functional theory (DFT) as implemented in the Crystal17 code. We report the effect of the computational parameters, i.e., the basis sets and exchange-correlation functional, on a selection of structures and show the robustness of the presented results. Next, we analyze the vibrational modes and intensities associated with the Raman peaks by distinguishing among pure phenyl, chain vibrations and mixed modes with ring and chain coupled motions. Finally, we discuss how the structural features could be used, or not, to calibrate Raman equipment, by comparison with available experimental data.

Our results are in good agreement with experimental data and we show that regardless the structural models used for polystyrene the main peaks in the spectra are reproduced and are due to phenyl ring vibrations. As expected, conformationally sensitive peaks are associated with pure chain or mixed ring and chain modes. Moreover, we find that finite length chains of polystyrene are essential to reproduce correctly the experimental spectra. In the following we described the methodology used in the calculations, then we discuss results for infinite PST chains and then we move to short oligomers. We finish the paper with discussion and conclusions.

II. Theoretical Methods

Calculations were performed using all-electron Gaussian-type basis set and Kohn-Sham Hamiltonian as implemented in the CRYSTAL17 code. Several exchange-correlation functional were used: PBE, PBE-D3 (with semi-classical corrections as proposed by Grimme to take into account dispersive interactions) and hybrid B3LYP. Split-valence basis sets of different quality available from Crystal database were adopted.

The numerical accuracy parameters in calculating the Coulomb and Hartree-Fock exchange series, defined by the truncation tolerances for bioelectronic integrals of Coulomb and exchange series, were set to 8 8 8 8 and 16, respectively. The threshold for the total energy

convergence of the self-consisted cycle was set to 10^{-11} Hartree. The exchange-correlation contribution was evaluated by numerical integration over the cell volume. The default integration grid (XLGRID) was adopted with 75 radial points and with a maximum number of 974 angular points in the regions relevant for chemical bonding.

Atom positions were fully relaxed by adopting default optimization algorithms with convergence criteria for atomic gradients recommended for vibrational calculations. For optimized structures, vibrational frequencies at the Gamma point were calculated using the harmonic approximation. The frequencies are evaluated as the eigenvectors of the mass-weighted Hessian matrix.

Raman intensities are computed by means of fully analytical approach that is based on a Coupled-Perturbed Hartree-Fock/Kohn-Sham (CPHF/KS) [55,56] approach for the response of the electronic density with respect to the external electric field. In this approach the Raman scattering intensity due to a Q_i vibrational mode of frequency ω_i, associated with an *xy* component of a polarizability tensor of an oriented single crystal is given by

$$I_{xy}^{i} \propto \left(\frac{\alpha_{xy}}{\partial Q_i}\right)$$

The powder (polycrystalline) Raman spectrum is obtained by averaging over the possible orientations of the single crystal [57]. The integrated intensities are normalized to the highest peak that is arbitrarily set to 1000. The convolution of the spectra is done automatically by Crystal17 with default parameters. Visualization of vibrational modes is done with CRYSPLOT [58]. Experimental spectra from refs. [50,51] are used to compare with.

STRUCTURAL MODELS OF POLYSTYRENE

Infinite trans-planar and helical chains

Figure 1 illustrates two structural models of infinite syndiotactic polystyrene (sPST) chains with trans-planar and helical configurations. These chains extend along the *c*-direction and in the trans-planar form the polymer chain has a regular *trans* (T)-planar (zigzag) conformation while in the helical form a regular repetition of *trans* (T) and *gauche* (G) conformations of the skeleton C-C bonds is present. Differences in the conformation of the carbon backbone result in the different orientations and relative positions of attached phenyl groups.

The sPST structural models employed in this study are based on the works of Torres *et al.*[50,51]. However, unlike previously, we do not impose any rod group symmetry constrains on atoms within the unit cell. Only the translational symmetry along the chain periodic direction is preserved. As a result, each unit cell is constructed such that it contains four phenyl rings and consists of a total 64 atoms.

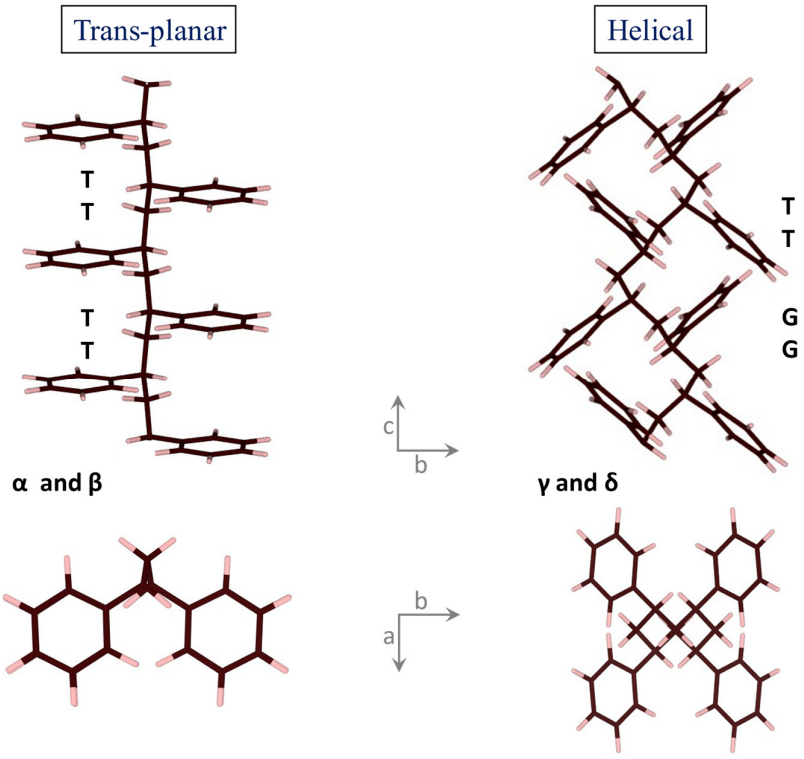

Figure 1. Structures of trans-planar and helical syndiotactic polystyrenes chains used in the calculations. C atoms in brown, H in pink. Trans-planar conformation is present in the α and β crystalline sPST phases and helical in the γ and δ phases.

Finite oligomers

Figure 2 depicts several sPTS-based oligomer structures that were considered:

1. the first structure was obtained by cutting a segment from the "infinite" trans-planar sPST. It contains four phenyl groups within the simulation cell and a "linear" carbon backbone chain, but the periodicity along the chain axis is no longer preserved.
2. the other two finite structures are based on models available at [59]. The first one is based on syndiotactic PST and consists of six phenyl rings with a bent carbon chain, while the second one exhibits a spiral-like arrangement of six phenyl rings with a distinct carbon chain geometry.

The dangling bonds at the ends of the carbon chains have been saturated by either adding a CH_3 group or an H atom to create a CH_2 group at the ends. All of the structures are either isolated polymers or oligomer in the vacuum. There are no periodic images to interact with.

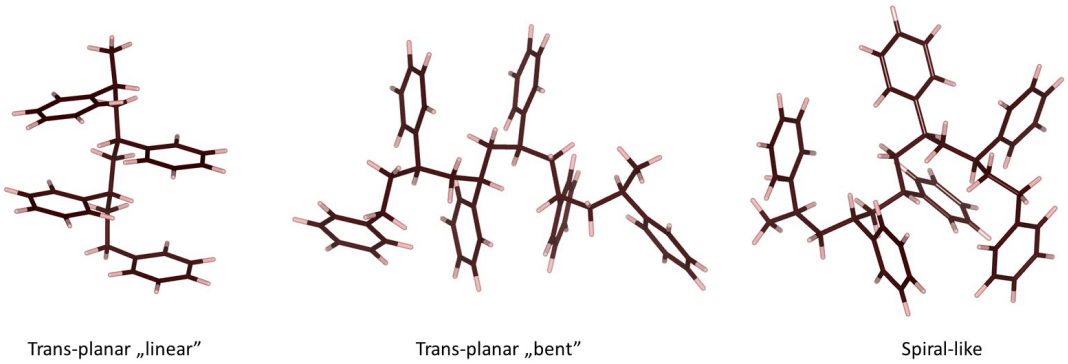

Figure 2. Oligomer finite structures.

III. RESULTS

Computational benchmark

The choice of basis set in Crystal17, which relies on Gaussian-type atomic orbitals, is crucial as it can affect the accuracy of calculated vibrational spectra. Therefore, a comprehensive investigation was conducted to assess the impact of the basis set and exchange-correlation functional on the Raman spectra of an isolated benzene molecule, which serves as the fundamental unit of a polystyrene structure. The obtained results were then compared with available experimental data. Next, selected computational settings were used to calculate the Raman spectra of infinite trans-planar and helical polystyrene chains. While the complete details of the benchmark study can be found in the Supplementary Information (SI), we will focus here on discussing the most significant findings.

The results obtained for benzene demonstrate an important dependence of the calculated Raman frequencies on both the basis set and the exchange-correlation functional (as visible in Tables S1 and S2 in the SI). When employing the hybrid B3LYP functional, the calculated frequencies tend to be shifted towards higher values (blue-shifted) compared to the results obtained with the PBE functional. Furthermore, the frequencies calculated using the B3LYP functional are generally overestimated with respect to the experimental data. In contrast, the PBE functional exhibits a better agreement with the experimental results, particularly for frequencies below 1700 cm^{-1}. These lower frequency vibrations primarily correspond to ring deformations, C-C stretching, and C-C-H bending motions. It is worth noting that the frequencies in the higher frequency region (above 3000 cm^{-1}), associated with C-H stretching vibrations, are significantly overestimated by both functionals when compared to experimental data. This overestimation can be attributed to the strong anharmonic nature of these vibrations, which was not accounted in the adopted level of theory. The seemingly better performance of the PBE functional in reproducing the experimental data can actually be misleading due to the lack of anharmonic effects.

Regarding the accuracy of frequency estimation, the introduced error varies depending on the computational setting as well as the atoms involved in the vibration and type of motion. Nonetheless, when examining the full computed Raman spectra, the overall spectral characteristics and the peaks relative intensities are alike, indicating a robustness with respect to the computational parameters (see Figure S1).

In the case of an infinite trans-planar polystyrene chain, we used selected basis sets and we included a PBE-D3 functional to account for the interactions between phenyl rings and the carbon backbone. For each computational configuration, the structure of polystyrene chain was fully optimized, and the relevant geometric parameters, such as bond angles and distances, are summarized in Table S3. The calculated repetition length along the *c*-axis falls within the range of 5.07 to 5.14 Å, which agrees well with experimental data for crystalline α/β sPST, where the repetition length is found to be in a range 5.06-5.1 Å[42].

Figure 3 illustrates the Raman spectra of trans-planar infinite polystyrene chain, obtained using different basis sets and functionals, divided into lower and higher frequency regions. Notably, the main spectral features are consistently reproduced across various computational settings. When employing the B3LYP functional, the calculated frequencies exhibit a blue shift compared to the PBE and PBE-D3 values, similar to what was observed for benzene molecule. The frequency differences between the PBE and PBE-D3 functionals, with respect to a specific basis set, are minimal. In the lower frequency region below 1700 cm^{-1}, slight shifts in peak positions can be observed among different basis sets (for a given functional), yet these shifts are small (up to 5-6 cm^{-1}) and can be partially attributed to variations in optimized bond distances and angles resulting from different computational settings.

The choice of basis set has a more significant impact on the relative intensities, with an overall increase in intensity observed for all functionals when Basis 5 is employed. However, the computed intensities must be treated with caution as they are highly sensitive to the choice of computational parameters. Furthermore, measured intensities are also subject to variations caused by factors such as the optical path, laser wavelength, and other experimental conditions. Consequently, due to inherent fluctuations in both computed and measured intensities, only a semi-quantitative comparison can be made between the two.

The higher frequency region of the spectra (2800-3300 cm^{-1}), corresponding to C-H stretching vibrations, exhibits a significantly higher sensitivity to the choice of computational parameters. For each of the employed functionals, the frequency shifts between the two basis sets used can reach up to 30 cm^{-1} and are accompanied by variations in the relative intensities. As already mentioned, the calculated intensities are subjected to some inaccuracies. Moreover, the C-H vibrations are influenced by strong anharmonic effects which were not included in the calculations. Therefore, the interpretation of the C-H region should be treated with caution.

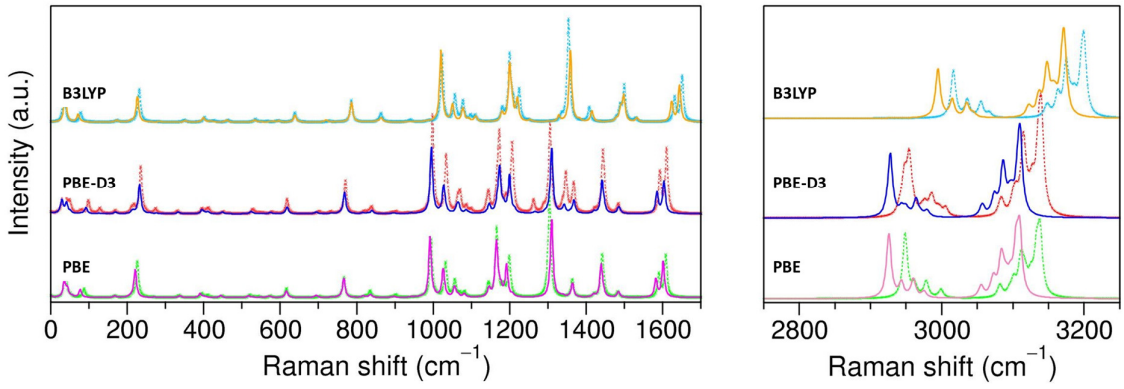

Figure 3. Raman spectra of trans-planar infinite polystyrene chain obtained with different functionals (PBE, PBE-D3 and B3LYP) and two different basis sets: Basis 5 in dotted lines and Basis 7 in solid lines (details of the basis sets can be found in the SI).

A similar benchmark was carried out as well for helical sPST, however, the B3LYP functional was not included. The calculated repetition length along the *c* direction for helical sPST is within the range of 7.7-7.9 Å (see Table S3), which is in excellent agreement with available experimental data for crystalline δ-sPST, where the *c* axis is equal to 7.7 Å[42]. Similarly, to the trans-planar infinite sPST, the Raman spectra of helical phase below 1700 cm^{-1} exhibits consistent behaviour regardless of the chosen basis set and functional, while more noticeable changes are observed in the C-H region (see Figure S2).

Irrespective of the computational settings employed, the main Raman spectral features for both infinite polymers are captured, ensuring the generality of the obtained results and conclusions. Therefore, our focus will be exclusively on the combination of the PBE-D3 functional with the Basis set 7. This particular combination not only yields geometrical parameters for infinite polystyrene chains that align perfectly with experimental data but also exhibits the smallest error in C-H stretch frequency when compared to experimental values[50,51].

In the following subsections, we will discuss the sensitivity of Raman spectra to different polystyrene configurations. Firstly, we will present a comparison between infinite trans-planar and helical polystyrene chains. Then, we will analyse the influence of finite chain length and oligomer structure. It is important to note that due to the frequency offset between calculated and experimental values, as well as the large number of calculated modes, comparison of Raman spectra is not straightforward, both within theoretical models and when comparing them to experimental data. To address this challenge, the visualization of vibrating atoms using CRYSPLOT was done. This allowed for distinguishing modes associated with the movement of phenyl rings, carbon chains, or mixed modes involving both, and enabling the assignment of the most intense peaks in the spectra to specific atoms. The mode description follows nomenclature used in ref.[50], where the superscript "*ch*" indicates carbon or hydrogen atoms belonging to the carbon chain, and "*ph*" indicates atoms of the phenyl group.

INFINITE POLYMER CHAINS: Trans-planar and helix PST

Figure 4 shows the Raman spectra for trans-planar and helix PST structures. To simplify the analysis, we divide the spectra in three regions: high frequency range above 2900 cm^{-1}, middle frequency region **between 1650-1040 cm^{-1}** and a low frequency region **below 1040** cm^{-1}. We discuss these regions separately, and we decompose vibrational modes into 3 groups that are either pure phenyl vibrations (“ph”), pure chain vibrations (”ch”) or a mixed modes coupling phenyl ring motion with carbon backbone. Tables S5 and S6 in the SI collect all the calculated frequencies with a given assignment, here we focus on the most important features. Figures S3 and S4 present visualization of chosen modes for trans-planar and helical sPTS, with arrows indicating atoms that are mostly contributing to the vibration.

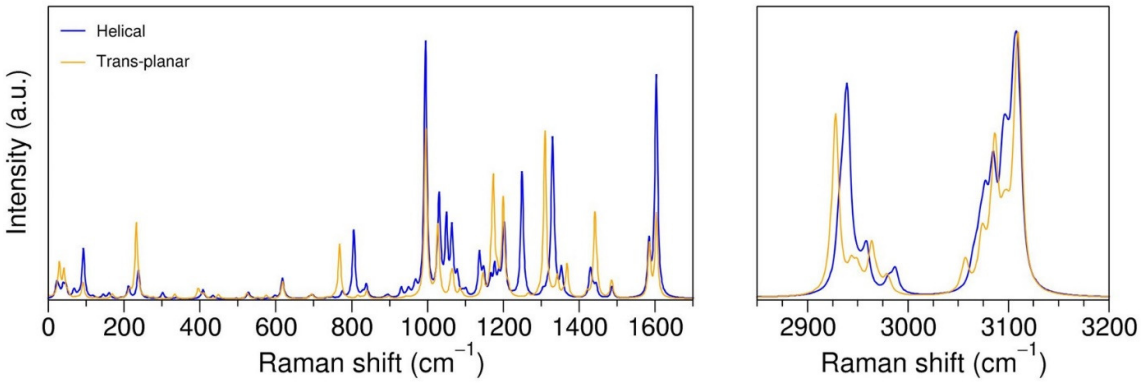

Figure 4. Calculated Raman spectra for infinite trans-planar and helical forms of syndiotactic polystyrene.

High frequency region above 2900 cm^{-1}: As previously mentioned, this part of the spectrum is related to the C-H stretching vibrations, which are strongly anharmonic in nature and are not well described by our calculations. As a result, the calculated frequencies are overestimated by approximately 50-60 cm^{-1} compared to experimental values.

The C-H vibrations can be separated into two groups based on C and H positions in the polystyrene:

- 2900-3000 cm^{-1} : C-H stretching vibrations in CH_2 and CH groups in the carbon chain
- 3050-3150 cm^{-1} : C-H stretching vibrations in the phenyl ring

It is important to highlight that these two groups of C-H vibrations are indeed well separated, with a noticeable gap in the range of 3000-3050 cm^{-1} where no peaks are found. However, this finding is inconsistent with experimental observations, as peaks in this region are typically observed in the experimental data. It should be noted that, the calculations do not reproduce the overtones and combination modes that can be present in the experimental spectra.

Middle frequency region 1650-1040 cm^{-1}: This particular region exhibits numerous distinct features, making the comparison between the trans-planar and helix PST structures quite complex. To simplify the analysis, we have subdivided the mid-frequency region into smaller zones where the spectra of the two PST polymorphs overlap or display clear differences. These zones, depicted in Figure 5, provide a focused view of the vibrational modes within each specific frequency range.

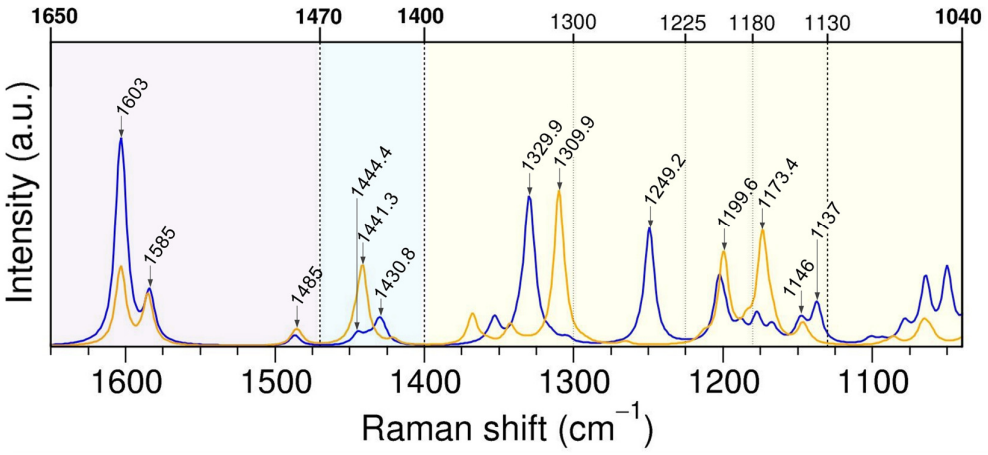

Figure 5. Comparison of Raman spectra of trans-planar and helical PST in the mid-frequency range. Helix PST in blue and trans-planar in orange

In the frequency range of **1650-1470 cm^{-1}**, a good match of the spectra of the trans-planar and helical configurations is observed. While the peak positions are in good agreement, some differences in the relative peaks intensities are present. Peaks in this range primarily correspond to vibrations of the phenyl rings and are not expected to be sensitive to the chain configuration. A strong peak around 1603 cm^{-1} is mainly characterized by the C^{ph}-C^{ph} stretching, and the in-plane bending motion of the H^{ph}-C^{ph}-C^{ph} atoms. The modes below 1600 cm^{-1} up to 1550 cm^{-1} couple in-plane motion of phenyl groups, i.e., C^{ph}-C^{ph} stretching and H^{ph}-C^{ph}-C^{ph} bending, with H^{ch}-C^{ch}-C^{ph} bending motion of the CH group from carbon chain and associated carbon atom from the phenyl ring. The modes found in the proximity of the small overlapping peak around 1485 cm^{-1} are due to in-plane motions of atoms in the phenyl ring, in particular H^{ph}-C^{ph}-C^{ph} bending, C^{ph}-C^{ph} and the C^{ph}-C^{ch} stretching. Selected modes from this range are schematically shown in Figures S3 and S4.

In the region **1400-1470 cm^{-1}** half of modes involves pure chain vibrations and the rest are complex modes that couple chain and phenyl ring motions. In the case of trans-planar PST, the most intense peak at 1441.30 cm^{-1} is dominated by H^{ch}-C^{ch}-H^{ch} bending motion in the CH_2 groups, that are vibrating in phase, with a minor contribution of the in-plane ring motion (see Figure S3). Below the 1441.30 cm^{-1} peak, the modes are mainly due to H^{ch}-C^{ch}-H^{ch} bending in CH_2 groups being in opposite phase. Above the 1441.30 cm^{-1} peak, the movements of CH/CH_2 groups and phenyl rings are strongly coupled. However, the intensities of the peaks around 1441.30 cm^{-1} are significantly lower.
In the case of the helix sPST, there is a clear peak splitting with lower peak composed of two intense modes at 1427.87 and 1430.80 cm^{-1}, and with higher peak including two intense vibrations at 1437.71 and 1444.42 cm^{-1}. The modes at 1427.87 cm^{-1}, 1430.80 cm^{-1} and 1437.71 cm^{-1} are due to bending motion in the CH_2 groups, while mode at 1444.42 cm^{-1} results from mixing of in-plane ring motion with CH group bending from the carbon backbone. In previous studies, it was shown that in the experimental Raman spectra of a helical crystalline phase a well-resolved doublet with maxima at 1451 and 1440 cm^{-1} is present and the splitting was attributed to bending of the so called external and internal CH_2 groups of the s(2/1)2 helix[51]. Indeed, visualization of the 1427.87 cm^{-1}, 1430.80 cm^{-1} and 1437.71 cm^{-1} vibrations has shown that lower frequency modes are due to bending motion in external CH_2 groups while higher frequency mode is associated with internal CH_2 groups. The

atoms involved in the vibrations are presented in the Figure S4. This proves that the peak splitting originates from the helical conformation of the PST chain.

The spectra in range from **1400 cm^{-1} to 1040 cm^{-1}** clearly depends on the sPST configuration and is dominated by complex modes that account for about 64% of modes in this zone for the trans-planar PST and for about 82% for helix PST (based on Tables S5 and S6). Nonetheless, pure phenyl ring or pure chain modes can be as well identified. The main features that can be distinguished are:

- **1400-1300 cm^{-1}** : the most intense peaks for the helix PST (1329.95 cm^{-1}) and the trans-planar PST (1309.88 cm^{-1}) result from a similar type of atomic motions, i.e., wagging of the CH and CH_2 groups along the carbon chain with some contribution from C-H wagging in the phenyl ring. The frequency offset for similar types of motion is probably due to the different orientations of the carbon chain for the two structures – the carbon backbone is linear for trans-planar PST, while for helix the backbone is bent, creating two orthogonal branches. Experimentally[50,51], in a similar frequency range, broad peaks of maximum intensity at 1319 cm^{-1} for the trans-planar and at 1339 cm^{-1} for the helical sPTS were found, which seem to be reproduced here.
- **1300-1225 cm^{-1}**: this region is dominated by CH/CH_2 wagging modes that can be coupled with ring vibrations. For trans-planar PST half of the modes in this region are pure chain modes; for helix PST only one pure chain mode is found, remaining modes are mixed vibrations. Most of the peaks in this region are of very low intensities, with the exception of the peak at 1249.21 cm^{-1} present for the helix PST. This mode is a mixture of CH/CH_2 wagging, C^{ch}-C^{ch}-C^{ch} bending and phenyl ring motion, i.e. H^{ph}-C^{ph}-C^{ph} bending, C^{ph}-C^{ph} stretching and C^{ph}-C^{ch} stretching. Similar features can be found as well in the experimental spectra[50,51], where peak at 1250 cm^{-1} appears only for a helical sPST.
- **1225-1180 cm^{-1}** : the most intense peaks for trans-planar PST (1199.61 cm^{-1}) and for helix PST (1202.77 cm^{-1}) are due to phenyl ring motions (H^{ph}-C^{ph}-C^{ph} bending and C^{ph}-C^{ph} stretching) coupled with chain motion (C^{ch}-C^{ph} stretching, C^{ph}-C^{ch}-H^{ch} bending, and small contribution from CH_2 wagging).
- **1180-1130 cm^{-1}** : for trans-planar PST, pure phenyl ring vibrations dominate in this region and are concentrated around 1146 cm^{-1} and 1168 cm^{-1}, but these modes have relatively small intensities and are suppressed by peak at 1173.67 cm^{-1} that couples chain CH_2 torsion-like motion along the carbon chain and CH group bending (H^{ch}-C^{ch}-C^{ph}) with H^{ph}-C^{ph}-H^{ph} bending from phenyl ring. The mode at 1152.18 cm^{-1} is a pure chain vibration with atoms from CH_2 group (less CH) moving along the carbon backbone. For helix PST pure phenyl ring modes are present around 1147 cm^{-1} and at 1166.60 cm^{-1}, the remaining modes are complex.
- **1130-1040 cm^{-1}**: In this part of the spectra only complex modes are found and there are too many of them to be discussed in detail.

Low frequency region below 1040 cm^{-1}: In this region, shown in the Figure 6, the majority of modes are complex. However, specific types of phenyl ring deformations can be still identified and these modes will be analyzed in more detail. The motion of phenyl groups can be categorized as an in-plane and out-of-plan ring deformations, which are schematically depicted in the Figure 7, and follow nomenclature from ref.[50].

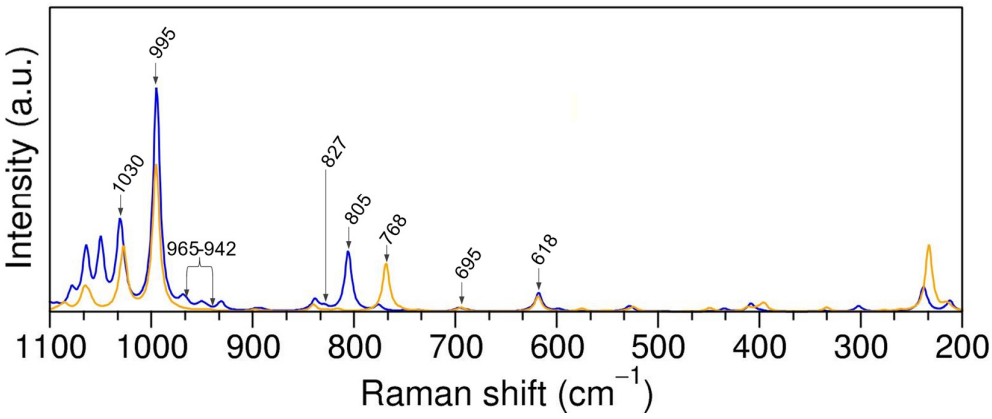

Figure 6. Comparison of Raman spectra of trans-planar and helical PST in the low-frequency range. Helix PST in blue and trans-planar in orange.

The peak observed around 1030 cm^{-1}, which overlaps in both trans-planar and helix PST configurations, is associated with breathing-like movement of the phenyl rings, labeled as the D_1 deformation. The calculated frequencies for this peak are precisely 1027.28 cm^{-1} for the trans-planar PST while for the helix PST, two closely spaced peaks with similar intensity are found at 1030.21 cm^{-1} and 1031.22 cm^{-1}. Following that, the next intense peak overlapping in both polymorphs occurs around 995 cm^{-1} and is characterized by in plane deformations of the phenyl ring, referred to as a D_2 deformation. Furthermore, the presence of peaks around 618 cm^{-1} in both PST configurations can be attributed to D_3-type deformations of the phenyl ring.

The out-of-plane ring deformations, denoted as D_4, D_5 or D_6 deformations, are found for trans-planar PST around frequencies 965-942 cm^{-1}, 827 cm^{-1} and 695 cm^{-1}. These type of deformations occur in similar frequency regions for helix PST, namely around frequencies 961 cm^{-1}, 945 cm^{-1}, 897 cm^{-1}, 833-823 cm^{-1} and 697-687 cm^{-1}. However, it is important to note that the intensities associated with the out-of-plane deformations (D_4, D_5, or D_6 modes) are much lower compared to the in-plane deformations of the phenyl ring.

The two prominent peaks observed at 768.33 cm^{-1} for trans-planar PST and at 805.70 cm^{-1} for helix PST align well with experimental observations in the 700-800 cm^{-1} region[48,49]. Experimentally, it was established that a strong, sharp peak at 773 cm^{-1} is associated with all-trans conformation of the carbon chain, while the peak at 798 cm^{-1} was attributed to the helical (mixed trans/gauche) conformation. These peaks were described as originating from symmetric breathing-like motion of phenyl groups. However, our analysis shows that these modes are rather attributed to the coupling of in-plane deformations of the phenyl rings (though not symmetric) with the chain motion. The involvement of the carbon skeleton in the vibration explains why the corresponding frequency is sensitive to the polystyrene chain configuration. The discussed modes are presented in the Figures S3 and S4. Overall, the theoretical results demonstrate that the trans-planar and helical configurations should produce distinct signal in the 700-800 cm^{-1} frequency range but rather due to involvement of carbon chain in the vibration.

The remaining modes in the frequency range 1040-600 cm^{-1} are dominated by complex vibrations that involve deformations of the phenyl ring and chain motions. These modes generally exhibit much lower intensities compared to the earlier discussed ones. Below 600 cm^{-1}, the vibrations are mostly due to collective motion of the entire polymer, although

some individual phenyl ring deformations can be identified. Nonetheless this part of the spectra won't be analyzed in more detail.

In summary, the vibrational modes that are sensitive to the configuration of PST primarily involve the carbon backbone or the coupling of motion between the carbon chain and phenyl rings. These modes are located in two main regions: 1040-1400 cm^{-1} and below 995 cm^{-1}. Notably, pure carbon chain modes are predominantly present within the range of 1135-1445 cm^{-1}. On the other hand, the modes associated with the vibrations of phenyl rings are relatively insensitive to the PST configuration. These modes can be found in the regions of 1485-1605 cm^{-1}, 995-1030 cm^{-1}, and around 618 cm^{-1}.

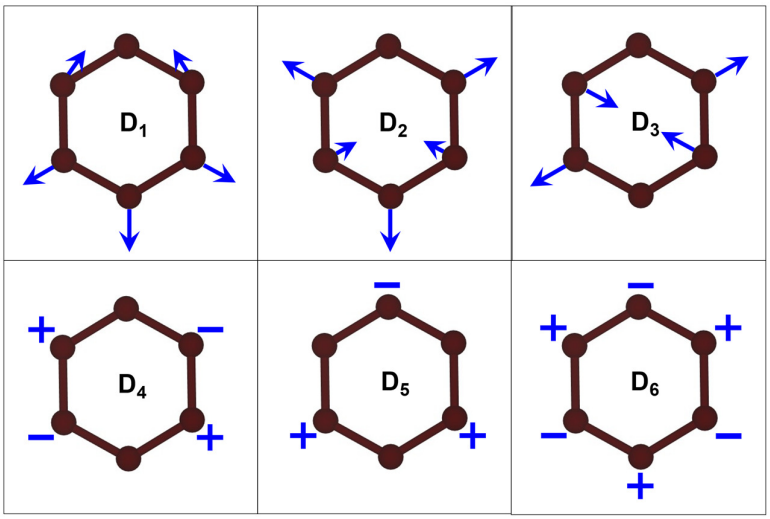

Figure 7. Schematical representation of the phenyl ring deformations. (+/-) indicate displacements perpendicular to the phenyl ring plane.

FINITE PST OLIGOMERS

Subsequently, the impact of the finite length of the polystyrene chain was investigated. Three models that were employed to represent sPST oligomers are depicted in the Figure 2, and include: i) Linear trans-planar PST, ii) Trans-planar PST with a bent carbon chain and iii) Spiral-like PST with different carbon chain geometry.

The Raman spectra of the oligomers are compared to that of the infinite trans-planar sPST in Figure 8. Regardless the PST model used, the overall shape of the Raman spectra is preserved, and the main features are reproduced. While the transition from infinite to finite linear trans-planar sPST introduces variations in the relative peak intensities and slight frequency shifts in conformationally sensitive regions (3200-2900 cm^{-1}, 1400-1040 cm^{-1}, and below 950 cm^{-1}), more significant changes occur when the oligomer structure becomes bent and the relative orientation of the phenyl groups is altered. Particularly, in the regions of 1400-1040 cm^{-1} and below 950 cm^{-1}, the reorientation of the rings and modifications in the oligomer shape lead to increased intensity of certain modes. Moreover, as the system's symmetry decreases from infinite to finite, a greater number of mixed modes emerge, leading to reduction of the pure chain vibrations (compare Tables S5-S8). The remaining pure chain modes are predominantly observed in the range of 1480-1420 cm^{-1}, although mixed modes are also present in this region.

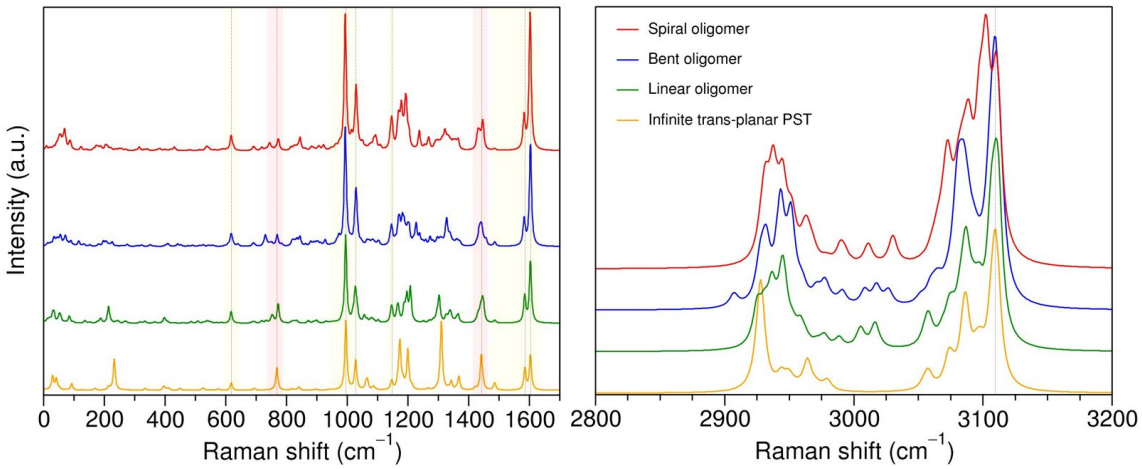

Figure 8. Calculated Raman spectra for short oligomers compared to the spectra of infinite trans-planar polystyrene chain. Yellow and red shades indicate main modes used as a reference peaks, where yellow color indicates pure phenyl ring vibrations while red corresponds to mixed or chain modes.

In contrast, variations in the sPST structure have a minimal impact on the pure vibrations of the phenyl rings, as the corresponding modes in the Raman spectra overlap across all PST configurations. These modes can be observed in the regions of 1625-1480 cm^{-1}, 1040-950 cm^{-1}, and around 618 cm^{-1}. Additionally, pure phenyl ring vibrations are also present in the region of 1480 cm^{-1} to 1490 cm^{-1}, although their intensity is relatively weaker compared to other phenyl ring vibrations. It is important to note that the relative intensities of the peaks associated with the phenyl groups vary depending on the specific configuration of the sPST, as they are clearly influenced by ring and chain orientations and changes in their interactions. For instance, the difference in intensity between peaks ~1585 cm^{-1} and ~1603 cm^{-1} increases when going from infinite PST to bent oligomers. In general, the intensity of these peaks increases across the structures and approaches the intense peak ~995 cm^{-1} while the intensity of the conformationally sensitive peaks in the region 1400-1040 cm^{-1} decreases.

In fact, a correction that includes temperature and laser wavelength can be applied for intensities to mimic the experimental conditions. It is important to highlight that the correction, as it is implemented in the Crystal17 code, only affects the intensities, not the vibrational frequencies. Figure S5 shows comparison of Raman spectra for infinite trans-planar sPST, both with and without intensity correction, alongside a bent oligomer with intensity correction. Clearly, the application of temperature correction has a significant impact on the relative intensities and seem to improve the agreement with the experimental spectra, particularly in terms of relative intensities of lower and higher frequency regions. Figure S6 highlights changes in the lower frequency region for various sPST models due to the intensity correction. Indeed, the relative intensities undergo modifications, with low-frequency modes (below 300 cm^{-1}) being magnified. The results also demonstrate that relative peak intensities within the range 400-1700 cm^{-1} match closer experimental data when finite oligomers are used instead of infinite sPST model. However, it should be kept in mind that calculated peak intensities are subject to inaccuracies and depend on the computational parameters, in particular on the basis set. Nonetheless, the general conclusions and comparisons made among all considered sPST models used should remain unaffected.

Figure 8 shows as well that the C-H stretching region is sensitive to changes in the local environment due to conformation of the polystyrene chain. Interestingly, in the frequency

range of 2990 cm^{-1} to 3050 cm^{-1}, new peaks emerge in the Raman spectra of oligomer structures, which were not observed in the infinite PST chains. Further analysis revealed that these new peaks correspond to the vibrations of the CH_3 and CH_2(Ph) terminating groups located at the ends of the oligomers. The contribution from end groups is also present in the 2900-2990 cm^{-1} region and in the lower frequency part, where carbon chain vibrations are expected. In the range between 3050 cm^{-1} and 2900 cm^{-1}, the CH_2/CH_3 end groups give rise to new peaks and contribute to significant changes in the relative peaks intensities. Above 3050 cm^{-1}, where C-H vibrations from the phenyl groups occur, the relative intensities are as well modified, but the general shape of the spectra and the overall spectral range remain relatively similar. However, it should be noted that the C-H region is not adequately described in the calculations, as mentioned previously. The calculated frequencies and relative intensities in this region are highly dependent on the chosen basis set and functional. As a result, a reliable qualitative analysis of the C-H region cannot be conducted.

IV. DISCUSSION

The Raman spectra of various model structures of syndiotactic polystyrene were compared, and it was observed that the essential characteristics of the spectra can be accurately reproduced regardless of the model used. This is because polymers, including polystyrene, are composed of numerous chemically identical units, each containing a relatively small number of atoms. As a result, the complexity of the infrared or Raman spectrum is significantly reduced. Furthermore, the modes associated with phenyl rings are unaffected by the conformation of the polymer chain, meaning that the stretching and bending modes of the rings remain independent of the chain structure.

Our results show that the geometry of the carbon backbone and the relative orientations of the phenyl rings primarily impact modes associated with chain or mixed vibrations. Reduction of polystyrene symmetry from infinite to finite chains and the presence of end groups lead to the appearance of new peaks in the spectra. Furthermore, the configuration of polystyrene also influences the relative intensities of peaks, including those associated with phenyl group vibrations.

A comprehensive comparison between trans-planar and helical forms of PTS revealed distinct regions in the Raman spectra where differences between the two structures are expected, in line with experimental findings. For instance, the experimentally observed peak splitting in the helical structure with maxima at 1440 and 1451 cm^{-1} was theoretically predicted to be around 1430 cm^{-1} and 1444 cm^{-1}. In the case of the trans-planar configuration, a broad peak at 1450 cm^{-1} was measured, and our calculations reproduced this single peak at 1441 cm^{-1}. The origin of the peak splitting in the helical phase was attributed to the different frequencies of bending motion in external and internal CH_2 groups. Experimentally, the presence of such a double peak has been used as an indicator of the of helical phase with mixed *trans* and *gauche* arrangements of the carbon chain, and our calculations support this assumption. However, it is important to take caution when interpreting theoretical predictions, as a similar splitting of the peak around 1444 cm^{-1} was also observed for a linear trans-planar oligomer when a different basis set was used (results not included).
Another interesting example is a sharp, intense peak calculated only for the helical sPST at 1249 cm^{-1}. This corresponds to the peak detected experimentally at 1250 cm^{-1}, which was also exclusively observed for the helical structure.
Indeed, the alignment between calculations and experimental data provides further evidence of the distinct Raman characteristics of the helical and trans-planar sPST configurations. It is

worth noting that the differences between the Raman spectra of the two phases are more pronounced in theory than in experiment. This observation underscores the importance of combining both theoretical and experimental approaches to gain a comprehensive understanding of the distinct behaviours exhibited by different sPST configurations.

Moving to short oligomers introduces additional features in the Raman spectra that were absent for infinite chains. Reducing the system's symmetry leads to the emergence of more mixed modes involving both carbon chain and phenyl ring motions, as well as changes due to chain end groups. This effect is particularly evident when comparing linear and bent oligomers. Altering the oligomer's geometry modifies the distances between the phenyl rings and the carbon chain, thereby affecting their interactions and polarizability. Consequently, peak intensities change, and more low-intensity peaks emerge in the spectra. Furthermore, the relative intensities of double peaks associated with phenyl ring vibrations in the regions of 1625-1550 cm^{-1} and 1040-995 cm^{-1} vary and for oligomer structures show better agreement with experimental spectra (particularly when the temperature correction is included for intensities, see Figure S5). However, it is important to note that the calculated relative intensities may not precisely match the experimental data and can be influenced by the chosen basis set and functional used in the calculations, as well as the temperature correction. Therefore, these intensities should be interpreted only at a semi-quantitative level. Similarly, experimental intensities are also prone to inaccuracies, as they can be affected by factors such as the laser used for measurements or the optical path.

The general shape of the calculated Raman spectra agrees well with experimental data, particularly in the lower frequency region, which is accurately reproduced by the theory. In the Table 1, we compare available experimental data for Raman active vibrations in polystyrene with calculated values. The experimental frequencies are taken from ASTM E1840-96 standard[60] and serve as a calibration reference for the Raman spectrometer [40]. The theoretical values correspond to various trans-planar sPST structures, including infinite chains as well as linear and bent oligomers. It is important to note that the absence of symmetry constraints in the calculations results in many computed frequencies, making direct comparisons challenging. To address this, the frequencies listed in the table were selected based on the overall agreement in the shape of the theoretical and experimental Raman spectra. For the theoretical values, a frequency range is provided that contains all computed values. The complete list of all frequencies can be found in the supplementary information (Table S9). The differences between the theoretical and experimental values range from 1 cm^{-1} to nearly 30 cm^{-1}, depending on the specific mode and type of atomic motion being considered.

The aim is to compare qualitatively experimental data with theory in order to investigate the nature of associated vibrations and access their stability with respect to structural modifications in polystyrene. Each frequency in the Raman spectra was assigned to the corresponding group of atoms responsible for the vibration, as indicated in the Table 1. The analysis revealed that the majority of modes used for calibration are associated with pure phenyl ring vibrations, which makes them relatively insensitive to changes in the polystyrene configuration. Importantly, the assignment of vibrating atoms remains consistent across all trans-planar PST structures, including infinite chain and finite oligomers, in the vicinity of the listed frequencies. Furthermore, two modes observed experimentally at 795.8 cm^{-1} and 1450.5 cm^{-1}, have corresponding theoretical vibrations that are either mixed modes or mixed/pure chain vibrations. It is possible then that these modes may experience frequency

shifts between different polystyrene samples/structures used in experiments, suggesting they may not be suited for calibration purposes.

Table 1. Experimental and theoretical (trans-planar model) frequencies for polystyrene. Experimental values are taken from ASTM E1840-96 standard and are used for the calibration. The group of atoms that are associated with a given mode are also indicated.

Exp. (cm^{-1})	Theo. Trans-planar PST (cm^{-1})			Assignment
	Infinite	"linear" oligomer	"bent" oligomer	
620.9	616.9-618.5	616.6-618.1	616.3-618.6	ring
795.8	768.0	772.5	769.4	mixed
1001.4	994.9-995.6	994.7-995.5	992.8-995.3	ring
1031.8	1027.3-1032.1	1026.2-1031.9	1027.3-1030.0	ring
1155.3	1145.0-1147.2	1145.6-1147.6	1145.1-1147.2	ring
1450.5	1420.8-1446.6	1424.0-1449.5	1426.1-1457.3	chain or mixed
1583.1	1584.1-1585.5	1583.3-1585.3	1581.1-1583.9	ring
1602.3	1602.7-1604.3	1602.4-1604.6	1601.2-1604.4	ring
2852.4	?	?	?	C-H-chain or end group
2904.5	?	?	?	C-H chain
3054.3	3105.9-3110.4	3106.1-3111.3	3101.6-3114.1	C-H ring

The error in the calculated C-H stretching vibration is more significant compared to the experimental data. This discrepancy is expected as the calculations did not include the anharmonic corrections required for this type of vibration. Furthermore, the C-H region of the spectra is highly sensitive to the calculation parameters and the specific configuration of polystyrene. As a result, the calculated spectra in the C-H region did not precisely match the experimental findings, making it difficult to accurately assign calculated values to each experimental peak.

An important observation is that the additional peaks appearing between the C-H stretching from the chain and C-H stretching from the ring regions are present in the theoretical spectra only when finite length oligomers are considered. Interestingly, these peaks are consistently present in the experimental spectra as well. This suggests that the experimental samples contain polystyrene chains of varying lengths, which contribute to the observed spectral features and these additional peaks can serve as indicators of finite chain lengths in polystyrene samples.

V. CONCLUSIONS

In this study, the Raman spectra of various polystyrene models were calculated chosen after assessment, the PBE-D3 exchange-correlation functional and a Gaussian-type basis set implemented in the Crystal17 code. An extensive benchmark of the computational parameters confirmed the general applicability and robustness of the results with respect to the choice of basis set and functional.

The comparison between trans-planar and helical forms of PST, revealed conformationally sensitive regions in good agreement with experimental observations. It was found that Raman spectra can exhibit sensitivity to the conformation of sPST and to either all-trans or mixed trans-gauche chains. However, the differences between trans-planar and helical sPST forms observed experimentally were more subtle compared to theoretical predictions and changes observed with infrared spectroscopy.

As complexity was gradually introduced into the models and the carbon backbone transitioned from infinite chain to finite-length oligomers, a mixing of chain and phenyl ring movements was observed. As a result additional peaks of relatively low intensity below 1700 cm^{-1} has emerged. On the other hand, the primary peaks associated with phenyl ring vibrations were present across all PST structures and only their relative intensities were modified. This indicates that further increase in the size of the oligomer models would not lead to significant changes in the spectra but rather we should expect appearance of mixed modes with low intensities in conformationally sensitive regions and modifications in relative peak's intensities.

Our calculations show that the peaks measured in the middle and low frequency region at 1602.3 cm^{-1}, 1583.1 cm^{-1}, 1155.3 cm^{-1}, 1031.8 cm^{-1}, 1001.4 cm^{-1}, 620.9 cm^{-1}, are robust as they come from phenyl ring vibrations and they could be used for calibration purposes. On the other hand, peaks at 1450.5 cm^{-1} and 795.8 cm^{-1} are dependent on the conformation of polystyrene as they correspond to chain or mixed modes.

Peaks in the higher frequency region, associated to C-H stretching vibrations, are overestimated as anharmonic effects are not included. Nonetheless, the investigation of polystyrene oligomers revealed that the finite-length chains of PST have to be considered to properly describe features in the C-H stretching region observed experimentally. The presence of end groups in polystyrene introduces changes in the stretching region of C-H atoms from the carbon backbone and leads to appearance of new peaks in the region between stretching of C-H from the chain and from the phenyl groups. These additional peaks are consistently visible in the experimental spectra, making our findings a valuable indicator of finite lengths of polystyrene chains.

In future studies, it would be worthwhile to explore the impact of tacticity or crystallinity on Raman spectra. The presence of crystallinity and intermolecular interactions among polystyrene chains may influence the configurationally sensitive regions in the Raman spectra, potentially leading to peak splitting or alterations in relative intensities. Investigating these effects could further enhance our understanding of the vibrational behaviour of polystyrene and its various configurations.

SUPPORTING INFORMATION: Supplementary materials include additional information about computational benchmark, visual representation of chosen vibrational modes for infinite polymers, tables with calculated vibrational frequencies.

The input and output files of the calculations for discussed polymer structures are available by NOMAD repository. The published calculations include PBE-D3 functional with Basis set 7, as defined in the SI. The data can be found either by dataset name (*CHARISMA-PST-2023*) or the dataset id number (*XXXXXXXXXX*). Additional data are available from the corresponding author, M.C., upon request. THIS HAVE TO BE MODIFIED AFTER PUBLISHING DATA ON NOMAD

ACKNOWLEDGEMENTS

This work was supported by the EU H2020 Project, "Characterisation and Harmonisation for Industrial Standardisation of Advanced Materials" (CHARISMA), under Grant Agreement no. 952921.

This project has received funding from the European Union's Horizon 2020 research and innovation programme under grant agreement No 814426 NanoInformaTIX (Development and Implementation of a Sustainable Modelling Platform for NanoInformatics).

This work was performed using HPC resources from GENCI- CINES/IDRIS (Grant 2022-x2022082131).

References

(1) Andrady, A. L.; Neal, M. A. Applications and Societal Benefits of Plastics. *Philos. Trans. R. Soc. B Biol. Sci.* **2009**, *364* (1526), 1977–1984. https://doi.org/10.1098/rstb.2008.0304.

(2) Akdogan, Z.; Guven, B. Microplastics in the Environment: A Critical Review of Current Understanding and Identification of Future Research Needs. *Environ. Pollut.* **2019**, *254*, 113011. https://doi.org/10.1016/j.envpol.2019.113011.

(3) Li, W. C.; Tse, H. F.; Fok, L. Plastic Waste in the Marine Environment: A Review of Sources, Occurrence and Effects. *Sci. Total Environ.* **2016**, *566–567*, 333–349. https://doi.org/10.1016/j.scitotenv.2016.05.084.

(4) Kedzierski, M.; Frère, D.; Le Maguer, G.; Bruzaud, S. Why Is There Plastic Packaging in the Natural Environment? Understanding the Roots of Our Individual Plastic Waste Management Behaviours. *Sci. Total Environ.* **2020**, *740*, 139985. https://doi.org/10.1016/j.scitotenv.2020.139985.

(5) Evode, N.; Qamar, S. A.; Bilal, M.; Barceló, D.; Iqbal, H. M. N. Plastic Waste and Its Management Strategies for Environmental Sustainability. *Case Stud. Chem. Environ. Eng.* **2021**, *4* (September). https://doi.org/10.1016/j.cscee.2021.100142.

(6) Peeken, I.; Primpke, S.; Beyer, B.; Gütermann, J.; Katlein, C.; Krumpen, T.; Bergmann, M.; Hehemann, L.; Gerdts, G. Arctic Sea Ice Is an Important Temporal Sink and Means of Transport for Microplastic. *Nat. Commun.* **2018**, *9* (1). https://doi.org/10.1038/s41467-018-03825-5.

(7) Dioses-Salinas, D. C.; Pizarro-Ortega, C. I.; De-la-Torre, G. E. A Methodological Approach of the Current Literature on Microplastic Contamination in Terrestrial Environments: Current

Knowledge and Baseline Considerations. *Sci. Total Environ.* **2020**, *730*, 139164. https://doi.org/10.1016/j.scitotenv.2020.139164.

(8) Lwanga, E. H.; Beriot, N.; Corradini, F.; Silva, V.; Yang, X.; Baartman, J.; Rezaei, M.; van Schaik, L.; Riksen, M.; Geissen, V. Review of Microplastic Sources, Transport Pathways and Correlations with Other Soil Stressors: A Journey from Agricultural Sites into the Environment. *Chem. Biol. Technol. Agric.* **2022**, *9* (1), 1–20. https://doi.org/10.1186/s40538-021-00278-9.

(9) Ashrafy, A.; Liza, A. A.; Islam, M. N.; Billah, M. M.; Arafat, S. T.; Rahman, M. M.; Rahman, S. M. Microplastics Pollution: A Brief Review of Its Source and Abundance in Different Aquatic Ecosystems. *J. Hazard. Mater. Adv.* **2023**, *9* (December 2022), 100215. https://doi.org/10.1016/j.hazadv.2022.100215.

(10) Frias, J. P. G. L.; Nash, R. Microplastics: Finding a Consensus on the Definition. *Mar. Pollut. Bull.* **2019**, *138* (September 2018), 145–147. https://doi.org/10.1016/j.marpolbul.2018.11.022.

(11) Gigault, J.; Halle, A. ter; Baudrimont, M.; Pascal, P. Y.; Gauffre, F.; Phi, T. L.; El Hadri, H.; Grassl, B.; Reynaud, S. Current Opinion: What Is a Nanoplastic? *Environ. Pollut.* **2018**, *235*, 1030–1034. https://doi.org/10.1016/j.envpol.2018.01.024.

(12) Cox, K. D.; Covernton, G. A.; Davies, H. L.; Dower, J. F.; Juanes, F.; Dudas, S. E. Human Consumption of Microplastics. *Environ. Sci. Technol.* **2019**, *53* (12), 7068–7074. https://doi.org/10.1021/acs.est.9b01517.

(13) Lim, X. Z. Microplastics Are Everywhere - but Are They Harmful? *Nature* **2021**, *593* (7857), 22–25. https://doi.org/10.1038/d41586-021-01143-3.

(14) Bhuyan, M. S. Effects of Microplastics on Fish and in Human Health. *Front. Environ. Sci.* **2022**, *10* (March), 1–17. https://doi.org/10.3389/fenvs.2022.827289.

(15) Kwon, J. H.; Kim, J. Y. J. W.; Pham, T. D.; Tarafdar, A.; Hong, S.; Chun, S. H.; Lee, S. H.; Kang, D. Y.; Kim, J. Y. J. W.; Kim, S. Bin; Jung, J. Microplastics in Food: A Review on Analytical Methods and Challenges. *Int. J. Environ. Res. Public Health* **2020**, *17* (18), 1–23. https://doi.org/10.3390/ijerph17186710.

(16) Yuan, Z.; Nag, R.; Cummins, E. Human Health Concerns Regarding Microplastics in the Aquatic Environment - From Marine to Food Systems. *Sci. Total Environ.* **2022**, *823*, 153730. https://doi.org/10.1016/j.scitotenv.2022.153730.

(17) Käppler, A.; Fischer, D.; Oberbeckmann, S.; Schernewski, G.; Labrenz, M.; Eichhorn, K. J.; Voit, B. Analysis of Environmental Microplastics by Vibrational Microspectroscopy: FTIR, Raman or Both? *Anal. Bioanal. Chem.* **2016**, *408* (29), 8377–8391. https://doi.org/10.1007/s00216-016-9956-3.

(18) Cowger, W.; Gray, A.; Christiansen, S. H.; DeFrond, H.; Deshpande, A. D.; Hemabessiere, L.; Lee, E.; Mill, L.; Munno, K.; Ossmann, B. E.; Pittroff, M.; Rochman, C.; Sarau, G.; Tarby, S.; Primpke, S. Critical Review of Processing and Classification Techniques for Images and Spectra in Microplastic Research. *Appl. Spectrosc.* **2020**, *74* (9), 989–1010. https://doi.org/10.1177/0003702820929064.

(19) Vinay Kumar, B.; Löschel, L. A.; Imhof, H. K.; Löder, M. G. J.; Laforsch, C. Analysis of Microplastics of a Broad Size Range in Commercially Important Mussels by Combining FTIR and Raman Spectroscopy Approaches. *Environ. Pollut.* **2021**, *269*, 116147. https://doi.org/10.1016/j.envpol.2020.116147.

(20) Brandt, J.; Bittrich, L.; Fischer, F.; Kanaki, E.; Tagg, A.; Lenz, R.; Labrenz, M.; Brandes, E.; Fischer, D.; Eichhorn, K.-J. High-Throughput Analyses of Microplastic Samples Using Fourier Transform Infrared and Raman Spectrometry. *Appl. Spectrosc.* **2020**, *74* (9), 1185–1197.

https://doi.org/10.1177/0003702820932926.

(21) Xu, J. L.; Thomas, K. V.; Luo, Z.; Gowen, A. A. FTIR and Raman Imaging for Microplastics Analysis: State of the Art, Challenges and Prospects. *TrAC - Trends Anal. Chem.* **2019**, *119*, 115629. https://doi.org/10.1016/j.trac.2019.115629.

(22) Gouadec, G.; Colomban, P. Raman Spectroscopy of Nanomaterials: How Spectra Relate to Disorder, Particle Size and Mechanical Properties. *Prog. Cryst. Growth Charact. Mater.* **2007**, *53* (1), 1–56. https://doi.org/10.1016/j.pcrysgrow.2007.01.001.

(23) Guo, H.; He, L.; Xing, B. Applications of Surface-Enhanced Raman Spectroscopy in the Analysis of Nanoparticles in the Environment. *Environ. Sci. Nano* **2017**, *4* (11), 2093–2107. https://doi.org/10.1039/c7en00653e.

(24) Hess, C. New Advances in Using Raman Spectroscopy for the Characterization of Catalysts and Catalytic Reactions. *Chem. Soc. Rev.* **2021**, *50* (5), 3519–3564. https://doi.org/10.1039/d0cs01059f.

(25) Chakraborty, I.; Banik, S.; Biswas, R.; Yamamoto, T.; Noothalapati, H.; Mazumder, N. Raman Spectroscopy for Microplastic Detection in Water Sources: A Systematic Review. *Int. J. Environ. Sci. Technol.* **2022**. https://doi.org/10.1007/s13762-022-04505-0.

(26) Hanlon, E. B.; Manoharan, R.; Koo, T. W.; Shafer, K. E.; Motz, J. T.; Fitzmaurice, M.; Kramer, J. R.; Itzkan, I.; Dasari, R. R.; Feld, M. S. Prospects for in Vivo Raman Spectroscopy. *Phys. Med. Biol.* **2000**, *45* (2). https://doi.org/10.1088/0031-9155/45/2/201.

(27) Allakhverdiev, E. S.; Khabatova, V. V.; Kossalbayev, B. D.; Zadneprovskaya, E. V.; Rodnenkov, O. V.; Martynyuk, T. V.; Maksimov, G. V.; Alwasel, S.; Tomo, T.; Allakhverdiev, S. I. Raman Spectroscopy and Its Modifications Applied to Biological and Medical Research. *Cells* **2022**, *11* (3). https://doi.org/10.3390/cells11030386.

(28) Prata, J. C.; Paço, A.; Reis, V.; da Costa, J. P.; Fernandes, A. J. S.; da Costa, F. M.; Duarte, A. C.; Rocha-Santos, T. Identification of Microplastics in White Wines Capped with Polyethylene Stoppers Using Micro-Raman Spectroscopy. *Food Chem.* **2020**, *331* (June), 127323. https://doi.org/10.1016/j.foodchem.2020.127323.

(29) Karami, A.; Golieskardi, A.; Choo, C. K.; Larat, V.; Karbalaei, S.; Salamatinia, B. Microplastic and Mesoplastic Contamination in Canned Sardines and Sprats. *Sci. Total Environ.* **2018**, *612*, 1380–1386. https://doi.org/10.1016/j.scitotenv.2017.09.005.

(30) Turner, S.; Horton, A. A.; Rose, N. L.; Hall, C. A Temporal Sediment Record of Microplastics in an Urban Lake, London, UK. *J. Paleolimnol.* **2019**, *61* (4), 449–462. https://doi.org/10.1007/s10933-019-00071-7.

(31) Allen, S.; Allen, D.; Phoenix, V. R.; Le Roux, G.; Durántez Jiménez, P.; Simonneau, A.; Binet, S.; Galop, D. Atmospheric Transport and Deposition of Microplastics in a Remote Mountain Catchment. *Nat. Geosci.* **2019**, *12* (5), 339–344. https://doi.org/10.1038/s41561-019-0335-5.

(32) Cho, S.; Kim, Y.; Chung, H. Feasibility Study for Simple On-Line Raman Spectroscopic Detection of Microplastic Particles in Water Using Perfluorocarbon as a Particle-Capturing Medium. *Anal. Chim. Acta* **2021**, *1165*, 338518. https://doi.org/10.1016/j.aca.2021.338518.

(33) Oßmann, B. E.; Sarau, G.; Holtmannspötter, H.; Pischetsrieder, M.; Christiansen, S. H.; Dicke, W. Small-Sized Microplastics and Pigmented Particles in Bottled Mineral Water. *Water Res.* **2018**, *141*, 307–316. https://doi.org/10.1016/j.watres.2018.05.027.

(34) Zhao, S.; Danley, M.; Ward, J. E.; Li, D.; Mincer, T. J. An Approach for Extraction, Characterization and Quantitation of Microplastic in Natural Marine Snow Using Raman Microscopy. *Anal. Methods* **2017**, *9* (9), 1470–1478. https://doi.org/10.1039/c6ay02302a.

(35) Domogalla-Urbansky, J.; Anger, P. M.; Ferling, H.; Rager, F.; Wiesheu, A. C.; Niessner, R.; Ivleva, N. P.; Schwaiger, J. Raman Microspectroscopic Identification of Microplastic Particles in Freshwater Bivalves (Unio Pictorum) Exposed to Sewage Treatment Plant Effluents under Different Exposure Scenarios. *Environ. Sci. Pollut. Res.* **2019**, *26* (2), 2007–2012. https://doi.org/10.1007/s11356-018-3609-3.

(36) Di, M.; Wang, J. Microplastics in Surface Waters and Sediments of the Three Gorges Reservoir, China. *Sci. Total Environ.* **2018**, *616–617*, 1620–1627. https://doi.org/10.1016/j.scitotenv.2017.10.150.

(37) Lv, L.; He, L.; Jiang, S.; Chen, J.; Zhou, C.; Qu, J.; Lu, Y.; Hong, P.; Sun, S.; Li, C. In Situ Surface-Enhanced Raman Spectroscopy for Detecting Microplastics and Nanoplastics in Aquatic Environments. *Sci. Total Environ.* **2020**, *728*, 138449. https://doi.org/10.1016/j.scitotenv.2020.138449.

(38) Fang, C.; Sobhani, Z.; Zhang, X.; Gibson, C. T.; Tang, Y.; Naidu, R. Identification and Visualisation of Microplastics/ Nanoplastics by Raman Imaging (Ii): Smaller than the Diffraction Limit of Laser? *Water Res.* **2020**, *183*, 116046. https://doi.org/10.1016/j.watres.2020.116046.

(39) Araujo, C. F.; Nolasco, M. M.; Ribeiro, A. M. P.; Ribeiro-Claro, P. J. A. Identification of Microplastics Using Raman Spectroscopy: Latest Developments and Future Prospects. *Water Res.* **2018**, *142*, 426–440. https://doi.org/10.1016/j.watres.2018.05.060.

(40) Ntziouni, A.; Thomson, J.; Xiarchos, I.; Li, X.; Bañares, M. A.; Charitidis, C.; Portela, R.; Lozano Diz, E. Review of Existing Standards, Guides, and Practices for Raman Spectroscopy. *Appl. Spectrosc.* **2022**, *76* (7), 747–772. https://doi.org/10.1177/00037028221090988.

(41) Baugh, L. S.; Schulz, D. N. Discovery of Syndiotactic Polystyrene: Its Synthesis and Impact. *Macromolecules* **2020**, *53* (10), 3627–3631. https://doi.org/10.1021/acs.macromol.0c00350.

(42) Gowd, E. B.; Tashiro, K.; Ramesh, C. Structural Phase Transitions of Syndiotactic Polystyrene. *Prog. Polym. Sci.* **2009**, *34* (3), 280–315. https://doi.org/10.1016/j.progpolymsci.2008.11.002.

(43) Schellenberg, J. *Syndiotactic Polystyrene: Synthesis, Characterization, Processing, and Applications*; 2009. https://doi.org/10.1002/9780470557006.

(44) Guerra, G.; Vitagliano, V. M.; De Rosa, C.; Petraccone, V.; Corradini, P. Polymorphism in Melt Crystallized Syndiotactic Polystyrene Samples. *Macromolecules* **1990**, *23* (5), 1539–1544. https://doi.org/10.1021/ma00207a050.

(45) De Rosa, C.; Guerra, G.; Petraccone, V.; Corradini, P. Crystal Structure of the α-Form of Syndiotactic Polystyrene. *Polym. J.* **1991**, *23* (12), 1435–1442. https://doi.org/10.1295/polymj.23.1435.

(46) De Rosa, C.; Rapacciuolo, M.; Guerra, G.; Petraccone, V.; Corradini, P. On the Crystal Structure of the Orthorhombic Form of Syndiotactic Polystyrene. *Polymer (Guildf).* **1992**, *33* (7), 1423–1428. https://doi.org/10.1016/0032-3861(92)90117-F.

(47) Woo, E. M.; Sun, Y. S.; Yang, C. P. Polymorphism, Thermal Behavior, and Crystal Stability in Syndiotactic Polystyrene vs. Its Miscible Blends. *Prog. Polym. Sci.* **2001**, *26* (6), 945–983. https://doi.org/10.1016/S0079-6700(01)00010-7.

(48) Kellar, E. J. C.; Galiotis, C.; Andrews, E. H. Raman Vibrational Studies of Syndiotactic Polystyrene. 1. Assignments in a Conformational/Crystallinity Sensitive Spectral Region. *Macromolecules* **1996**, *29* (10), 3515–3520. https://doi.org/10.1021/ma950772t.

(49) Kellar, E. J. C.; Evans, A. M.; Knowles, J.; Galiotis, C.; Andrews, E. H. Raman Vibrational Studies of Syndiotactic Polystyrene. 2. Use of the Fundamental ν1 Vibrational Mode as a

Quantitative Measure of Crystallinity within Isotropic Material. *Macromolecules* **1997**, *30* (8), 2400–2407. https://doi.org/10.1021/ma961136d.

(50) Torres, F. J.; Civalleri, B.; Pisani, C.; Musto, P.; Albunia, A. R.; Guerra, G. Normal Vibrational Analysis of a Trans-Planar Syndiotactic Polystyrene Chain. *J. Phys. Chem. B* **2007**, *111* (23), 6327–6335. https://doi.org/10.1021/jp072257q.

(51) Torres, F. J.; Civalleri, B.; Meyer, A.; Pellegrino Musto; Albunia, A. R.; Rizzo, P.; Guerra, G. Normal Vibrational Analysis of the Syndiotactic Polystyrene s(2/1)2 Helix. *J. Phys. Chem. B* **2009**, *113* (15), 5059–5071. https://doi.org/10.1021/jp809043w.

(52) Kobayashi, M.; Nakaoki, T.; Ishihara, N. Polymorphic Structures and Molecular Vibrations of Syndiotactic Polystyrene. *Macromolecules* **1989**, *22* (11), 4377–4382. https://doi.org/10.1021/ma00201a037.

(53) Rastogi, S.; Goossens, J. G. P.; Lemstra, P. J. An in Situ SAXS/WAXS/Raman Spectroscopy Study on the Phase Behavior of Syndiotactic Polystyrene (SPS)/Solvent Systems: Compound Formation and Solvent (Dis)Ordering. *Macromolecules* **1998**, *31* (9), 2983–2998. https://doi.org/10.1021/ma9712920.

(54) Rastogi, S.; Gupta, V. D. Normal Vibrations and Their Dispersion in Syndiotactic Polystyrene. *J. Macromol. Sci. Part B* **1994**, *33* (2), 129–141. https://doi.org/10.1080/00222349408248083.

(55) Ferrero, M.; Rérat, M.; Orlando, R.; Dovesi, R. Coupled Perturbed Hartree-Fock for Periodic Systems: The Role of Symmetry and Related Computational Aspects. *J. Chem. Phys.* **2008**, *128* (1), 014110. https://doi.org/10.1063/1.2817596.

(56) Maschio, L.; Kirtman, B.; Rérat, M.; Orlando, R.; Dovesi, R. Ab Initio Analytical Raman Intensities for Periodic Systems through a Coupled Perturbed Hartree-Fock/Kohn-Sham Method in an Atomic Orbital Basis. I. Theory. *J. Chem. Phys.* **2013**, *139* (16). https://doi.org/10.1063/1.4824442.

(57) Prosandeev, S. A.; Waghmare, U.; Levin, I.; Maslar, J. First-Order Raman Spectra of AB′1⁄2B″1⁄2O3 Double Perovskites. *Phys. Rev. B* **2005**, *71* (21), 214307. https://doi.org/10.1103/PhysRevB.71.214307.

(58) *CRYSPLOT*. https://crysplot.crystalsolutions.eu/.

(59) University of Liverpool. *Polystyrene (PS)*. https://www.chemtube3d.com/_polystyrenef/.

(60) *ASTM E1840 − 96 Standard Guide for Raman Shift Standards for Spectrometer Calibration*; 2014.